Inorg. Chem. **2005**, *44*, 2018–2030

Coumarin-Based Chemosensors for Zinc(II): Toward the Determination of the Design Algorithm for CHEF-Type and Ratiometric Probes

Nathaniel C. Lim,[†] Jolene V. Schuster,[†] Maura C. Porto,[†] Maria A. Tanudra,[‡] Lili Yao,[‡] Hedley C. Freake,[‡], and Christian Brückner*[,†]

Department of Chemistry, University of Connecticut, Storrs, Connecticut 06269-3060, and Department of Nutritional Sciences, University of Connecticut, Storrs, Connecticut 06269-4017

Received August 9, 2004

The synthesis of a series of coumarin-based chemosensor assemblies for zinc is detailed, using established and novel synthetic pathways. Variations of the nature of the chelating unit (DPA or cyclen), position of the attachment point of the chelating unit (3- or 4-position), and nature of the 7-substituent (–OH, –OAc, or $–NR_2$) on the coumarin play a crucial role in whether, and to what extent, a CHEF-type or ratiometric response of the chemosensor is observed. Solvent effects are also discussed. The chemosensors were shown to be competent for detecting zinc pools in cultured rat pituitary (GH3) and hepatoma (H4IIE) cell lines. The work further defines the design algorithms for zinc-selective CHEF-type and ratiometric chemosensors.

Introduction

Perhaps thousands of proteins contain zinc. The pronounced Lewis-acid characteristics of the Zn^{2+} ion, its single redox state, and the flexibility and kinetic lability of its coordination sphere are responsible for its broad biological utility in catalytic and structural functions.[1] Whereas much is known about the structural chemistry of zinc,[2] the description of the spatial and temporal distribution patterns of zinc during biological events has only recently begun.[3,4,5] For instance, histochemical studies of mammalian tissues have revealed that the distribution patterns of labile zinc pools are affected in some types of prostate cancer and during ischemic shock, and zinc has been implied to function as a mediator of neuronal cell death.[4,6−9] Insulin is costored with zinc in secretory vesicles in pancreatic β-cells.[10,11] The modulation of the zinc concentration in pituitary tumor cells affects thyroid hormone regulation of gene expression.[12−14] Despite this rapidly growing body of knowledge, the homeostatic control or precise functions of zinc in these tissues or even within simpler single-cell organisms remain poorly understood.

The knowledge gap between the structural chemistry of zinc and zinc homeostasis and action is, at least in part, due to the lack of techniques for tracking Zn^{2+} in biological systems. This has led to the emergence of zinc-specific molecular sensors.[15−19] Molecular sensors or chemosensors

* Author to whom correspondence should be addressed. E-mail: c.bruckner@uconn.edu. Fax: +(860) 486-2981. Tel: +(860) 486-2743.
[†] Department of Chemistry.
[‡] Department of Nutritional Sciences.

(1) (a) Prasad, A. S. *Biochemistry of Zinc*; Plenum Press: New York, 1993. (b) Vallee, B. L.; Falchuk, K. H. *Physiol. Rev.* **1993**, *73*, 79−118.
(2) Auld, D. S. *Biometals* **2001**, *14*, 271−313.
(3) For recent reviews, see e.g.: (a) Sandstead, H. H.; Frederickson, C. J.; Penland, J. G. *J. Nutr.* **2000**, *130*, 496S−502S. (b) Maret, W. *BioMetals* **2001**, *14*, 187−190. (c) Takeda, A. *BioMetals* **2001**, *14*, 343−351
(4) Burdette, S. C.; Lippard, S. J. *Coord. Chem. Rev.* **2001**, *216−217*, 333−361.
(5) Finney, L. A.; O'Halloran, T. V. *Science* **2003**, *300*, 931−936.
(6) Koh, J. Y.; Suh, S. W.; Gwag, B. J.; He, Y. Y.; Hsu, C. Y.; Choi, D. W. *Science* **1996**, *272*, 1013−1016.
(7) Burdette, S. C.; Lippard, S. J. *Proc. Natl. Acad. Sci. U.S.A.* **2003**, *100*, 3605−3610.
(8) Frederickson, C. J.; Burdette, S. C.; Frederickson, C. J.; Sensi, S. L.; Weiss, J. H.; Yin, H. Z.; Balaji, R. V.; Truong-Tran, A. Q.; Bedell, E.; Prough, D. S.; Lippard, S. J. *J. Neurosci. Methods* **2004**, *139*, 79−89.
(9) Woodroofe, C. C.; Masalha, R.; Barnes, K. R.; Frederickson, C. J.; Lippard, S. J. *Chem. Biol.* **2004**, *11*, 1659−1666.
(10) Qian, W.-J.; Aspinwall, C. A.; Battiste, M. A.; Kennedy, R. T. *Anal. Chem.* **2000**, *72*, 711−717.
(11) Gee, K. R.; Zhou, Z.-L.; Qian, W.-J.; Kennedy, R. *J. Am. Chem. Soc.* **2002**, *124*, 776−778.
(12) Chattopadhyay, S.; Freake, H. C. *Mol. Cell Endocrinol.* **1998**, *136*, 151−157, 1998.
(13) Sciaudone, M.; Chattopadhyay, S.; Freake, H. C. *J. Nutr.* **2000**, *130*, 158−163.
(14) Sciaudone, M. P.; Yao, L.; Schaller, M.; Zinn, S. A.; Freake, H. C. *Biol. Trace Elem. Res.* **2004**, *99*, 219−231.
(15) Lim, N. C.; Freake, H. C.; Brückner, C. *Chem.—Eur. J.* **2005**, *11*, 38−49.
(16) Kimura, E.; Aoki, S. *BioMetals* **2001**, *14*, 191−204.
(17) Kimura, E.; Koike, T. *Chem. Soc. Rev.* **1998**, *27*, 179−184.
(18) Jiang, P.; Guo, Z. *Coord. Chem. Rev.* **2004**, *248*, 205−229.

10.1021/ic048905r CCC: $30.25
Published on Web 02/12/2005

are molecules capable of transforming chemical information such as the presence of a specific metal ion into an analytically useful signal.[20] A metal ion chemosensor comprises a metal ion recognition and a signal transduction domain that is triggered upon metal ion binding. For instance, metal binding triggers intense fluorescence of the sensor while the unbound molecule is nonfluorescent.[21] Such sensors have become known as CHEF (chelation-enhanced fluorescence)-type sensors.

The use of cell-permeable chemosensors allows the detection of zinc pools in live cells by means of fluorescence microscopy.[10,11,15,22−34] Total zinc levels within tissues are reasonably high (200 μM), but virtually all of this zinc is bound to proteins with high affinity. Free zinc levels in mammalian cells are generally extremely low, perhaps in the fM range, although recent estimates vary widely.[35,36] On the contrary, vesicles in the presynaptic terminals of mossy fiber terminals of the hippocampus have been found to achieve zinc concentrations of ∼200−300 μM.[37] Further, the successful imaging of vesicular zinc pools in a range of mammalian cells using sensors with μM binding constants for zinc[18,31] leads to the conclusion that a number of as yet ill-defined "imageable zinc" pools exist in which the concentration of zinc must be higher than the fM concentrations of free zinc in the cytosol derived from thermodynamic considerations.[35,36]

The first generation chemosensors of zinc, Zinquin and analogues, belong to the family of aminoquinolines.[26,38−47] Though they have proven their utility to probe a number of biological events,[38,43,48−51] their solubility and photophysical characteristics are not ideal.[52] This inspired the recent evolution of chemosensors for zinc. For some of these systems, no biological data were reported.[53] Most significantly, however, Lippard and collaborators,[9,23,25,28−30,32,54−56] Tsien,[23,25] O'Halloran,[22,34] Kennedy,[10,11] and Gee[27,57] and co-workers have recently introduced a new generation of sensors based on fluorescein and rhodamine chromophores conjugated to

(19) Kikuchi, K.; Komatsu, K.; Nagano, T. *Curr. Opin. Chem. Biol.* **2004**, *8*, 182−191.

(20) For recent reviews on chemosensor design and action, see e.g.: (a) *Fluorescent Chemosensors for Ion and Molecular Recognition*; Czarnik, A. W., Ed.; American Chemical Society: Washington, DC, 1992. (b) Czarnik, A. W. *Acc. Chem. Res.* **1994**, *27*, 302−308. (c) Fabrizzi, L.; Poggi, A. *Chem. Soc. Rev.* **1995**, 197−202. (d) Tsien, R. Y. In *Calcium as a Cellular Regulator*; Carafoli, E., Klee, C., Eds.; Oxford University Press: New York, 1999; pp 28−54. (e) de Silva, A. P.; Gunaratne, H. Q. N.; Gunnlaugsson, T.; Huxley, A. J. M.; McCoy, C. P.; Rademacher, J. T.; Rice, T. E. *Chem. Rev.* **1997**, *97*, 1515−1566. (f) de Silva, A. P.; Fox, D. B.; Huxley, H. J. M.; Moody, T. S. *Coord. Chem. Rev.* **2000**, *205*, 41−57. (g) Rurack, K.; Resch-Genger, U. *Chem. Soc. Rev.* **2002**, *31*, 116−127.

(21) Kavarnos, G. J. *Fundamentals of Photoinduced Electron Transfer*; VCH: Weinheim, Germany, 1993.

(22) Nasir, M. S.; Fahrni, C. J.; Suhy, D. A.; Kolodsick, K. J.; Singer, C. P.; O'Halloran, T. V. *J. Biol. Inorg. Chem.* **1999**, *4*, 775−783.

(23) Walkup, G. K.; Burdette, S. C.; Lippard, S. J.; Tsien, R. Y. *J. Am. Chem. Soc.* **2000**, *122*, 5644−5645.

(24) Qian, W.-J.; Kennedy, R. T. *Biochem. Biophys. Res. Commun.* **2001**, *286*, 315−321.

(25) Burdette, S. C.; Walkup, G. K.; Springler, B.; Tsien, R. Y.; Lippard, S. J. *J. Am. Chem. Soc.* **2001**, *123*, 7831−7841.

(26) Pearce, D. A.; Jotterand, N.; Carrico, I. S.; Imperiali, B. *J. Am. Chem. Soc.* **2001**, *123*, 5160−5161.

(27) Sensi, S. L.; Ton-That, D.; Weiss, J. H.; Rothe, A.; Gee, K. R. *Cell Calcium* **2003**, *34*, 281−284.

(28) Burdette, S. C.; Frederickson, C. J.; Bu, W.; Lippard, S. J. *J. Am. Chem. Soc.* **2003**, *125*, 1778−1787.

(29) Clark, M. A.; Duffy, K.; Timbrewala, J.; Lippard, S. J. *Org. Lett.* **2003**, *5*, 2051−2054.

(30) Woodroofe, C. C.; Lippard, S. J. *J. Am. Chem. Soc.* **2003**, *125*, 11458−11459.

(31) Lim, N. C.; Yao, L.; Freake, H. C.; Brückner, C. *Bioorg. Med. Chem. Lett.* **2003**, *13*, 2251−2254.

(32) Chang, C. J.; Jaworski, J.; Nolan, E. M.; Sheng, M.; Lippard, S. J. *Proced. Natl. Acad. Sci. U.S.A.* **2004**, *101*, 1129−1134.

(33) Chang, C. J.; Nolan, E. M.; Jaworski, J.; Burdette, S. C.; Sheng, M.; Lippard, S. J. *Chem. Biol.* **2004**, *11*, 202−210.

(34) Taki, M.; Wolford, J. L.; O'Halloran, T. V. *J. Am. Chem. Soc.* **2004**, *126*, 712−713.

(35) Hitomi, Y.; Outten, C. E.; O'Halloran, T. V. *J. Am. Chem. Soc.* **2001**, *123*, 8614−8615.

(36) Outten, C. E.; O'Halloran, T. V. *Science* **2001**, *292*, 2488−2492.

(37) Budde, T.; Minta, A.; White, J. A.; Kay, A. R. *Neuroscience* **1997**, *79*, 347−358.

(38) Zalewski, P. D.; Forbes, I. J.; Betts, W. H. *Biochem. J.* **1993**, *296*, 403−408.

(39) Mahadevan, I. B.; Kimber, M. C.; Lincoln, S. F.; Tiekink, E. R. T.; Ward, A. D.; Betts, W. H.; Forber, I. J.; Zalewski, P. D. *Aust. J. Chem.* **1996**, *49*, 561−568.

(40) Hendrickson, K. M.; Rodopoulos, T.; Pittet, P.-A.; Mahadevan, I.; Lincoln, S. F.; Ward, A. D.; Kurucsev, T.; Duckworth, P. A.; Forbes, I. J.; Zalewski, P. D.; Betts, W. H. *J. Chem. Soc., Dalton Trans.* **1997**, 3879−3882.

(41) Walkup, G. K.; Imperiali, B. *J. Am. Chem. Soc.* **1997**, *119*, 3443−3450.

(42) Walkup, G. K.; Imperiali, B. *J. Org. Chem.* **1998**, *63*, 6727−6731.

(43) Fahrni, C. J.; O'Halloran, T. V. *J. Am. Chem. Soc.* **1999**, *121*, 11448−11458.

(44) Kimber, M. C.; Mahadevan, I. B.; Lincoln, S. F.; Ward, A. D.; Tiekink, E. R. T. *J. Org. Chem.* **2000**, *65*, 8204−8209.

(45) Bronson, R. T.; Bradshaw, J. S.; Savage, P. B.; Fuangswasdi, S.; Lee, S. C.; Krakowiak, K. E.; Izatt, R. M. *J. Org. Chem.* **2001**, *66*, 4752−4758.

(46) Jotterand, N.; Pearce, D. A.; Imperiali, B. *J. Org. Chem.* **2001**, *66*, 3224−3228.

(47) Hendrickson, K. M.; Geue, J. P.; Wyness, O.; Lincoln, S. F.; Ward, A. D. *J. Am. Chem. Soc.* **2003**, *125*, 3889−3895.

(48) Frederickson, C. J.; Kasarskis, E. J.; Ringo, D.; Frederickson, R. E. *J. Neurosci. Methods* **1987**, *20*, 91−103.

(49) Zalewski, P. D.; Forbes, I. J.; Seamark, R. F.; Borlinghaus, R.; Betts, W. H.; Lincoln, S. F.; Ward, A. D. *Chem. Biol.* **1994**, *1*, 153−61.

(50) Coyle, P.; Zalewski, P. D.; Philcox, J. C.; Forbes, I. J.; Ward, A. D.; Lincoln, S. F.; Mahadevan, I.; Rofe, A. M. *Biochem. J.* **1994**, *303*, 781−786.

(51) Truong-Tran, A. Q.; Ho, L. H.; Chai, F.; Zalewski, P. D. *J. Nutr.* **2000**, *130*, 1459S-1466S.

(52) The chromophore is also relatively dim, with a fluorescence quantum yield of only 10%, combined with a low extinction coefficient ϵ of 10×10^3 M^{-1} cm^{-1}. It is not soluble in purely aqueous systems and often requires cosolvents such as DMSO for its application. Further, it requires a relatively short excitation wavelength of 350−370 nm, raising the concern of UV-induced cell damage. This $\lambda_{max-excitation}$ is also outside of the range of commonly available fluorescence microscopes (typical $\lambda_{excitation}$ = 450−490 nm).

(53) For a representative selection, see: (a) Ibrahim, R.; Tsuchiya, S.; Ogawa, S. *J. Am. Chem. Soc.* **2000**, *122*, 12174−12185. (b) Hirano, T.; Kikuchi, K.; Urano, Y.; Higuchi, T.; Nagano, T. *Angew. Chem., Int. Ed.* **2000**, *39*, 1052−1054. (c) Hirano, T.; Kikuchi, K.; Urano, Y.; Higuchi, T.; Nagano, T. *J. Am. Chem. Soc.* **2000**, *122*, 12399−12400. (d) Klein, G.; Kaufmann, D.; Schürch, S.; Reymond, J.-L. *Chem. Commun.* **2001**, 561−562. (e) Goodall, W.; Williams, J. A. G. *Chem. Commun.* **2001**, 2514−2515. (f) Jiang, P.; Chen, L.; Lin, J.; Liu, Q.; Ding, J.; Gao, X.; Guo, Z. *Chem. Commun.* **2002**, 1424−1425. (g) Gunnlaugsson, T.; Lee, T. C.; Parkesh, R. *Org. Biomol. Chem.* **2003**, *1*, 3265−3267. (h) Wu, Z.; Chen, Q.; Yang, G.; Xiao, C.; Liu, J.; Yang, S.; Ma, J. S. *Sens. Actuators B* **2004**, *99*, 511−515. (i) Bencini, A.; Berni, E.; Bianchi, A.; Fornasari, P.; Giorgi, C.; Lima, J. C.; Lodeiro, C.; Melo, M. J.; de Melo, J. S.; Parola, A. J.; Pina, F.; Pina, J.; Valtancoli, B. *Dalton Trans.* **2004**, 2180−2187. (j) Chen, Y.; Zeng, D. X. *ChemPhysChem* **2004**, *5*, 564−566.

(54) Burdette, S. C.; Lippard, S. J. *Inorg. Chem.* **2002**, *41*, 6816−6823.

(55) Chang, C. J.; Nolan, E. M.; Jaworski, J.; Okamoto, K.-I.; Hayashi, Y.; Sheng, M.; Lippard, S. J. *Inorg. Chem.* **2004**, *43*, 6774−6779.

(56) Nolan, E. M.; Lippard, S. J. *Inorg. Chem.* **2004**, *43*, 8310−8317.

(57) Gee, K. R.; Zhou, Z.-L.; Ton-That, D.; Sensi, S. L.; Weiss, J. H. *Cell Calcium* **2002**, *31*, 245−251.

picolylamines, aminocarboxylate, and cyclen chelating groups. The prime advantage of these sensors lies in the use of bright and relatively long-wavelength absorption/emission chromophores, and many have been shown to be suitable for interrogating zinc flux during biological events.[9,11,22,27,28,32,33,57] Despite their proven utility, these families of stains also have limitations. Some show only relatively weak fluorescence enhancements upon zinc binding (e.g. 3.1-fold for Zinpyr-1, 6-fold for Zinpyr-2, 5-fold for Zinpyr-4, 1.4- to 4.5-fold for the Zinspy family),[23,25,28,33,56] some exhibit an affinity for zinc which is many orders of magnitude less than that of Zinquin, and many sensors are sensitive toward proton-induced interfering fluorescence enhancement.[33,58] Thus, there is a strong need for the continued improvement in the chemosensor designs.

We introduced a zinc-selective coumarin-based CHEF-type chemosensor suitable for use in biological systems.[31] We also contributed to the development of a ratiometric sensor,[59] a much coveted goal.[30,32,34,54,57,60,61] Ratiometric chemosensors potentially allow the measurement of absolute zinc concentrations.[62] In this contribution we provide the full disclosure of our findings presented in our communications. Further, we report on the biological evaluation of the sensors previously not tested in cell cultures, extend the cell types tested, and provide further insight into the design paradigms for ratiometric sensors.

Experimental Section

Instruments and Materials. All solvents and reagents were used as received. Coumarin bromide **3**, bis(2-picolyl)amine (DPA), and 1,4,7,10-tetraazacyclododecane (cyclen) are commercially available (Acros, Aldrich, Strem). Known compounds **7**[63] and **12**[64] were prepared as described previously.

The analytical TLC plates were aluminum backed Silicycle ultrapure silica gel 60, 250 μm, while the flash column silica gel (standard grade, 60 Å, 32−63 mm) used was provided by Sorbent Technologies. ^{1}H and ^{13}C NMR spectra were recorded on a Bruker DRX400. The NMR spectra are expressed on the δ scale and were referenced to residual solvent peaks or internal TMS. UV−vis spectra were recorded on a Cary 50 spectrophotometer, fluorescence spectra on a Cary Eclipse, and IR spectra on a Thermo Nicolet Nexus 670. Melting points were determined on a Thomas-Hoover capillary melting point apparatus and are reported uncorrected. ESI mass spectra were recorded on a Micromass Quattro II at the UConn Department of Chemistry. High-resolution FAB mass spectra were provided by the Mass Spectrometry Facility, Department of Chemistry and Biochemistry, University of Notre Dame. Elemental analyses were provided by Numega Resonance Labs Inc., San Diego, CA. The purity of the compounds for which no elemental analysis was available was, based on their NMR spectra, judged to be better than 97% (see Supporting Information).

Preparation of 6,7-Dimethoxy-4-(1,4,7,10-tetraazacyclododec-1-ylmethyl)chromen-2-one (4). Cyclen (0.295 g, 1.17 mmol) was dissolved in CH_2Cl_2 (20 mL), and Na_2CO_3 (1.5 g) was added. A solution of 4-(bromomethyl)-6,7-dimethoxycoumarin (**3**) (0.563 g, 1.1 equiv, in 60 mL of CH_2Cl_2) was added dropwise. The resulting solution was stirred at ambient temperature under N_2 for 4 d. The solids were filtered off, and the filtrate was taken to dryness by rotary evaporation, yielding a yellow solid. The solid was dissolved in H_2O (30 mL) and four times extracted with CH_2Cl_2 (25 mL each). Evaporation of the combined organic phases yielded **4** (0.400 g, 60% yield): mp = 95−98 °C; ^{1}H NMR (DMSO-d_6, 400 MHz, δ) 7.24 (s, 1H), 7.06 (s, 1H), 6.43 (s, 1H), 4.02 (s, 2H), 3.86 (s, 6H), 2.97−2.82 (m, 16H) ppm; ^{13}C NMR (DMSO-d_6, 100 MHz, δ) 160.4, 152.6, 149.0, 145.7, 111.6, 110.9, 105.8, 100.2, 56.3, 56.2, 50.0 (br), 43.3 ppm; IR (KBr) ν_{max} 2830 (br), 1713 (s), 1614 (m), 1561 (m), 1517 (s), 1452 (s), 1421 (s), 1388 (m), 1280 (s), 1236 (s), 1156 (s), 1060 (m), 999 (m), 933 (m), 858 (m) cm^{-1}; MS (ES+, 100% CH_3OH, 30 V) m/z = 391 (MH^+); MS (FAB+, NBA) m/z = 391 (MH^+, 83%); HR-MS (FAB+ of MH^+, NBA; m/z) calcd for $C_{20}H_{31}N_4O_4$ 391.2345, found 391.2339.

Preparation of [4-((6,7-Dimethoxy-2-oxo-2*H*-chromen-4-yl)-methyl)-7,10-bis(ethoxycarbonylmethyl)-1,4,7,10-tetraazacyclododec-1-yl]acetic Acid Ethyl Ester (5). To a CH_2Cl_2/EtOH solution (10 mL/2 mL) containing **4** (0.220 g, 0.56 mmol) and Na_2CO_3 (0.480 g) was added ethyl bromoacetate (0.310 g, 3.3 equiv). The resulting solution was stirred at ambient temperature under N_2 for 3 d. The solids were filtered off, and the filtrate was taken to dryness by rotary evaporation, yielding a yellow residue. The residue was redissolved in CH_2Cl_2 and extracted twice with 1M HCl (20 mL each). Rotary evaporation of the aqueous phase afforded **5** as yellow solid (0.35 g, 80% yield): R_f = 0.38 (silica−CH_2Cl_2/10% MeOH); mp = 170−175 °C (dec); ^{1}H NMR (D_2O, 400 MHz, δ) 7.26 (s, 1H), 7.11 (s, 1H), 6.70 (br s, 1H), 4.45−2.70 (m, 36H), 1.36−1.32 (m, 9H) ppm; ^{13}C NMR (D_2O, 100 MHz, D1 = 5 s, δ) 167.2 (br), 162.7, 153.0, 149.3, 146.2, 113.9, 111.3, 104.5, 100.3, 63.7, 62.9, 62.3, 56.4, 53.6−47.6 (br, N−CH_2), 13.4, 13.3 ppm; IR (KBr) ν_{max} 3395 (br), 2980 (br), 1725 (s), 1614 (m), 1556 (m), 1519 (m), 1463 (s), 1423 (s), 1379 (s), 1283 (s), 1240 (s), 1157 (s), 1086 (m), 1027 (m), 999 (m), 874 (m) cm^{-1}; MS (ES+, 100% CH_3OH, 30 V) m/z = 649 (MH^+); MS (FAB+, NBA) m/z = 649 (MH^+, 97%), 671 (MNa^+, 37%); HR-MS (FAB+ of MH^+, NBA; m/z) calcd for $C_{32}H_{49}N_4O_{10}$ 649.3449, found 649.3456.

Preparation of 4-[(Bis(pyridin-2-ylmethyl)amino)methyl]-6,7-dimethoxychromen-2-one (6). 4-(Bromomethyl)-6,7-dimethoxycoumarin (**3**) (0.168 g, 0.56 mmol) was added to CH_2Cl_2 (20 mL) containing DPA (0.1 mL, 0.56 mmol) and Na_2CO_3 (0.350 g, 3.33 mmol). Once all the starting material was consumed (~24 h, monitored by TLC), the mixture was filtered. The resulting solution was taken to dryness by rotary evaporation, and **6** was isolated using column chromatography (silica−petroleum ether/85% EtOAc followed by CH_2Cl_2/5% MeOH) as light yellow solid (0.230 g, 90% yield): R_f = 0.22 (silica−CH_2Cl_2/5% MeOH); mp = 155−158 °C; ^{1}H NMR ($CDCl_3$, 400 MHz, δ) 8.54 (d, J = 4.1 Hz, 2H), 7.68−7.64 (m, 2H), 7.45 (d, J = 7.8 Hz, 2H), 7.31 (s, 1H), 7.20−7.17 (m, 2H), 6.82 (s, 1H), 6.60 (s, 1H), 3.94 (s, 3H), 3.90 (s, 9H) ppm; ^{13}C NMR ($CDCl_3$, 100 MHz, δ) 161.8, 158.7, 153.2, 152.9, 149.9, 149.4, 146.2, 136.9, 123.4, 122.6, 112.4, 111.5, 106.0, 100.1, 60.9, 56.7, 56.5, 55.7 ppm; IR (KBr) ν_{max} 3006 (w) 2932 (w), 2816 (w), 1718 (s), 1612 (m), 1589 (m), 1562 (m), 1515 (m), 1458 (m), 1422 (s), 1385 (m), 1277 (s), 1234 (s), 1199 (m), 1148 (m), 1060 (m), 994 (m), 918 (m), 852 (m) cm^{-1}; MS (ES+, 100% CH_3CN, 30 V) m/z = 418 (MH^+); MS (FAB+, NBA) m/z = 418 (MH^+,

(58) Aoki, S.; Kaido, S.; Fujioka, H.; Kimura, E. *J. Inorg. Chem.* **2003**, *42*, 1023−1030.
(59) Lim, N. C.; Brückner, C. *Chem. Commun.* **2004**, 1094−1095.
(60) Sclarafani, J. A.; Maratano, M. T.; Sisk, T. M.; Van Arman, S. A. *Tetrahedron Lett.* **1996**, *37*, 2193−2196.
(61) Henary, M. M.; Wu, Y.; Fahrni, C. J. *Chem.—Eur. J.* **2004**, *10*, 3015−3025.
(62) Lakowicz, J. R. *Principles of Fluorescence Spectroscopy*; 2nd ed.; Kluwer Academic/Plenum: New York, 1999.
(63) Sugino, T.; Tanaka, K. *Chem. Lett.* **2001**, *30*, 110−111.
(64) Van Gompel, J.; Schuster, G. B. *J. Org. Chem.* **1987**, *52*, 1465−1468.

53%); HR-MS (FAB+ of MH^+, NBA; *m*/*z*) calcd for $C_{24}H_{24}N_3O_4$ 418.1767, found 418.1774. Anal. Calcd for $C_{24}H_{23}N_3O_4$: C, 69.05; H, 5.55; N, 10.07. Found: C, 69.07; H, 5.53; N, 10.26.

Preparation of 3-(1-Hydroxyethyl)chromen-2-one (8). 3-Acetylchromen-2-one (**7**) (1.0 g, 5.3 mmol) was dissolved in THF (15 mL), and $CeCl_3$ (1.31 g, 1 equiv) was added. The mixture was cooled to 0 °C, and $NaBH_4$ (0.200 g, 1 equiv) was slowly added. Once all the starting material was consumed, the excess $NaBH_4$ was quenched with water. The product was then extracted into CH_2Cl_2. Rotary evaporation of the organic layer yielded crude **8** as a yellow oil (0.830 g, 82% yield): $R_f = 0.57$ (silica−CH_2Cl_2/5% MeOH); ^{1}H NMR (DMSO-d_6, 400 MHz, δ) 8.02 (s, 1H), 7.78−7.76 (m, 1H), 7.57−7.55 (m, 1H), 7.40−7.32 (m, 2H), 4.72−4.69 (m, 1H), 1.33 (d, $J = 6.4$ Hz, 3H) ppm.

Preparation of 3-(1-bromoethyl)chromen-2-one (9). Crude chromen-2-one **8** (0.80 g, 4.2 mmol) was dissolved in benzene (15 mL), and PBr_3 (1.42 g, 1.25 equiv) was added. Once all the starting material was consumed (∼2 h, monitored by TLC), the reaction mixture was washed thrice with 1 M NaOH (10 mL each). Rotary evaporation of the organic layer yielded crude **9** as a white solid (0.66 g, 62% yield): $R_f = 0.38$ (silica−CH_2Cl_2); ^{1}H NMR (DMSO-d_6, 400 MHz, δ) 8.36 (s, 1 H), 7.80−7.78 (m, 1H), 7.65−7.62 (m, 1H), 7.44−7.36 (m, 2H), 5.38 (q, $J = 7.0$ Hz, 1H), 2.02 (d, $J = 7.0$ Hz, 3H) ppm.

Preparation of 3-[1-(1,4,7,10-Tetraazacyclododec-1-yl)ethyl]-chromen-2-one Tetrahydrochloride (10). To a CH_2Cl_2 solution (20 mL) containing crude chromen-2-one **9** (0.30 g, 1.19 mmol) were added Na_2CO_3 (1.0 g) and cyclen (0.20 g, 1 equiv). The resulting solution was stirred at ambient temperature under N_2 for 2 h. The solids were filtered off, and the filtrate was extracted thrice with 2 M HCl (10 mL each). Rotary evaporation of the aqueous phase afforded **10** as a white solid (0.54 g, 93% yield): mp = 222−225 °C (dec); ^{1}H NMR (DMSO-d_6, 400 MHz, δ) 8.15 (s, 1H), 7.78 (d, $J = 7.0$ Hz, 1H), 7.63−7.58 (m, 1H), 7.38 (q, $J = 6.9$ Hz, 2H), 4.29 (s, 1H), 3.37−3.15 (br s, 16H), 1.48 (s, 3H) ppm; ^{13}C NMR (DMSO-d_6, 100 MHz, δ) 161.8, 152.8, 141.6, 131.7, 128.7, 126.6, 124.5, 119.1, 115.9, 50.4, 43.6, 42.0 ppm; IR (KBr) ν_{max} 2953 (br), 2652 (br), 1709 (s), 1608 (s), 1572 (m), 1455 (s), 1279 (m), 1189 (s), 961 (m) cm^{-1}; MS (FAB+, NBA) *m*/*z* = 345 (MH^+, 40%); HR-MS (FAB+ of MH^+, NBA; *m*/*z*) calcd for $C_{19}H_{29}N_4O_2$ 345.2291, found 345.2295.

Preparation of 3-(10-Oxo-2,3,5,6-tetrahydro-1*H*,4*H*,10*H*-11-oxa-3a-azabenzo[*de*]anthracen-9-yl)acrylic Acid Ethyl Ester (13). Hydroxyquinoline carbaldehyde **12** (2.08 g, 9.57 mmol) was dissolved in EtOH (24 mL). Diethyl glutaconate (1.78 mL, 10.06 mmol, 1.05 equiv) was added followed by 3 drops of piperidine (dried over KOH pellets), and the solution was refluxed for 24 h. The reaction mixture was allowed to slowly cool to room temperature and then chilled to −20 °C. The orange crystals deposited were filtered off and dried to yield **13** (3.06 g, 94% yield): R_f = 0.59 (silica−CH_2Cl_2/5% CH_3CN); mp = 180−185 °C (dec); ^{1}H NMR (DMSO-d_6, 400 MHz, δ) 8.17 (s, 1H), 7.49 (d, $J = 15.8$ Hz, 1H), 7.04 (s, 1H), 6.74 (d, $J = 15.8$ Hz, 1H), 4.16 (q, $J = 7.1$ Hz, 2H) 3.30 (m, 4H), 2.67 (m, 4H), 1.89 (m, 4H), 1.24 (t, $J = 7.1$ Hz, 3H) ppm; ^{13}C NMR (DMSO-d_6, 100 MHz, δ) 166.7, 159.8, 151.1, 147.3, 145.6, 139.9, 126.2, 119.0, 116.7, 111.3, 107.8, 104.9, 59.7, 49.5, 49.0, 26.7, 20.6, 19.7, 19.6, 14.2 ppm; IR (KBr) ν_{max} 2942 (m), 2843 (m), 1714 (s), 1695 (s), 1561 (m), 1524 (s), 1444 (m), 1374 (m), 1315 (s), 1275 (s), 1195 (s), 1162 (s), 1096 (m), 1040 (m), 990 (m), 801 (m) cm^{-1}; MS (ES+, 100% CH_3CN, 30 V) *m*/*z* = 339 (M^+); MS (FAB+, NBA) *m*/*z* = 339 (M^+, 40%); HR-MS (FAB+ of M^+, NBA; *m*/*z*) calcd for $C_{20}H_{21}NO_4$ 339.1471, found 339.1465.

Preparation of 10-Oxo-2,3,5,6-tetrahydro-1*H*,4*H*,10*H*-11-oxa-3a-azabenzo[*de*]anthracene-9-carbaldehyde (14). Acrylic acid ethyl ester **13** (3.55 g, 10.46 mmol) was dissolved in THF (300 mL) and water (10 mL). A freshly prepared OsO_4 solution in pyridine (2.66 mL of a 0.393 M solution, made by dissolving 1.0 g of OsO_4 in enough pyridine to make a 10 mL solution) was added to the suspension. The suspension was stirred at room temperature for 1 h, followed by addition of $NaIO_4$ (4.92 g, 23 mmol). Once the starting material was consumed (∼5 d), the solution was taken to dryness by rotary evaporation. The resulting solid was slurried in CH_2Cl_2, and the mixture washed with water. The organic layer was isolated and taken to dryness by rotary evaporation. Column chromatography (silica−CH_2Cl_2) was used to isolate **14** as an orange solid (1.65 g, 59%): $R_f = 0.25$ (silica−CH_2Cl_2/5% CH_3CN); mp = 190−195 °C (dec); ^{1}H NMR (DMSO-d_6, 400 MHz, δ) 9.87 (s, 1H), 8.23 (s, 1H), 7.25 (s, 1H), 3.39 (m, 4H), 2.69 (m, 4H), 1.89 (m, 4H) ppm; ^{13}C NMR (DMSO-d_6, 100 MHz, δ) 186.9, 161.0, 153.2, 149.3, 145.4, 128.6, 119.8, 111.6, 107.4, 105.1, 49.8, 49.3, 26.7, 20.4, 19.5, 19.4 ppm; IR (KBr) ν_{max} 2931 (m), 2849 (m), 1716 (s), 1675 (m), 1619 (s), 1582 (s), 1560 (m), 1514 (s), 1444 (m), 1350 (m), 1309 (s), 1285 (s), 1215 (m), 1186 (m), 1162 (m) cm^{-1}; MS (ES+, 100% CH_3CN, 30 V) *m*/*z* = 270 (MH^+); MS (FAB+, NBA) *m*/*z* = 269 (M^+, 78%), 270 (MH^+, 88%); HR-MS (FAB+ of MH^+, NBA; *m*/*z*) calcd for $C_{16}H_{16}NO_3$ 270.1130, found 270.1129. Anal. Calcd for $C_{16}H_{15.5}NO_{3.25}$ (**14**·0.25H_2O): C, 70.19; H, 5.71; N, 5.12. Found: C, 70.19; H, 5.55; N, 5.33.

Preparation of 9-[(Bis(pyridin-2-ylmethyl)amino)methyl]-2,3,5,6-tetrahydro-1*H*,4*H*-11-oxa-3a-azabenzo[*de*]anthracen-10-one (15). Aldehyde **14** (0.185 g, 0.69 mmol) was dissolved in 1,2-dichloroethane (20 mL). DPA (0.12 mL, 0.67 mmol) was added followed by $NaBH(OAc)_3$ (0.290 g, 1.37 mmol). The reaction was stirred for 24 h at ambient temperature. Saturated aqueous Na_2CO_3 (8 mL) was added to quench excess reductant, and the mixture was vigorously stirred for 30 min. The mixture was partitioned, and the aqueous layer extracted twice with CH_2Cl_2 (5 mL each). The combined organic extracts were washed with brine (10 mL) and dried over $MgSO_4$. The solvent was removed by rotary evaporation, and **15** was isolated using column chromatography (silica−solvent gradient, from CH_2Cl_2/20% CH_3CN, to CH_2Cl_2/40% CH_3CN, to CH_2Cl_2/5% MeOH) as a brown solid (0.280 g, 92% yield): $R_f = 0.13$ (silica−CH_2Cl_2/5% MeOH); mp = 87−93 °C; ^{1}H NMR ($CDCl_3$, 400 MHz, δ) 8.52 (d, $J = 4.8$ Hz, 2H), 7.71 (s, 1H), 7.64 (m, 4H), 7.13 (m, 2H), 6.87 (s, 1H), 3.92 (s, 4H), 3.66 (s, 2H), 3.25 (q, $J = 5.5$ Hz, 4 H), 2.88 (t, $J = 6.4$ Hz, 2H), 2.76 (t, $J = 6.4$ Hz, 2H), 1.98 (m, 4H) ppm; ^{13}C NMR ($CDCl_3$, 100 MHz, δ) 162.8, 159.5, 151.0, 149.0, 145.4, 141.9, 136.4, 124.8, 122.8, 121.9, 118.2, 117.4, 108.5, 106.4, 60.1, 53.2, 49.9, 49.6, 27.5, 21.5, 20.6, 20.3 ppm; IR (KBr) ν_{max} 2938 (br), 1712 (s), 1609 (s), 1569 (s), 1517 (m), 1473 (m), 1435 (s), 1353 (m), 1309 (s), 1167 (s), 1048 (m), 995 (m) cm^{-1}; MS (ES+, 100% CH_3CN, 30 V) *m*/*z* = 453 (MH^+); MS (FAB+, NBA) *m*/*z* 453 (MH^+, 10%); HR-MS (FAB+ of MH^+, NBA; *m*/*z*) calcd for $C_{28}H_{29}N_4O_2$ 453.2291, found 453.2299.

Preparation of 3-(7-Hydroxy-2-oxo-2*H*-chromen-3-yl)acrylic Acid Ethyl Ester (17). 2,4-Dihydroxybenzaldehyde (0.74 g, 5.36 mmol) was dissolved in EtOH (15 mL). Diethyl glutaconate (1.0 mL, 5.65 mmol) was added, followed by 3 drops of piperidine (dried over KOH pellets), and the solution was reflux for 24 h. The reaction mixture was then allowed to slowly cool to room temperature and then chilled to −20 °C. The yellow crystals formed were filtered off and dried to yield **17** (1.24 g, 89% yield): R_f = 0.47 (silica−CH_2Cl_2/5% CH_3CN); mp = 227−229 °C; ^{1}H NMR

(DMSO-d_6, 400 MHz, δ) 10.90 (br s, 1H), 8.44 (s, 1H), 7.56 (d, J = 8.6 Hz, 1H), 7.51 (d, J = 15.9 Hz, 1H), 6.86 (d, J = 16.0 Hz, 1H), 6.84 (dd, J = 8.2, 2.2 Hz, 1H), 6.74 (d, J = 2.2 Hz, 1H), 4.18 (q, J = 7.1 Hz, 2H), 1.25 (t, J = 7.1 Hz, 3H) ppm; ^{13}C NMR (DMSO-d_6, 100 MHz, δ) 166.7, 163.3, 159.7, 155.8, 145.9, 139.3, 131.3, 120.2, 116.7, 114.5, 112.0, 102.4, 60.5, 14.6 ppm; IR (KBr) ν_{max} 3321 (br), 1706 (s), 1598 (s), 1565 (m), 1448 (s), 1381 (m), 1293 (s), 1264 (m), 1203 (s), 1165 (m), 1001 (m), 870 (m) cm^{-1}; MS (FAB+, NBA) m/z = 260 (M^+, 7%), 261 (MH^+, 10%); HR-MS (FAB+ of MH^+, NBA; m/z) calcd for $C_{14}H_{13}O_5$ 261.0763, found 261.0745.

Preparation of 3-(7-Acetoxy-2-oxo-2*H*-chromen-3-yl)acrylic Acid Ethyl Ester (18). Phenol **17** (0.200 g, 0.77 mmol) was dissolved in dry pyridine (4 mL), and acetic anhydride (4 mL) was added. The reaction was stirred at ambient temperature for 0.5 h, was then poured onto ice, and was stirred for an additional 10 min. The resulting white precipitate was filtered and dried yielding **18** (0.210 g, 90%): R_f = 0.89 (silica−CH_2Cl_2/20% CH_3CN); mp = 153−157 °C; ^{1}H NMR (DMSO-d_6, 400 MHz, δ) 8.56 (s, 1H), 7.78 (d, J = 8.5 Hz, 1H), 7.55 (d, J = 16.0 Hz, 1H), 7.33 (d, J = 2.0 Hz, 1H), 7.21 (dd, J = 8.5, 2.1 Hz, 1H), 6.94 (d, J = 16.0 Hz, 1H), 4.20 (q, J = 7.1 Hz, 2H), 1.26 (t, J = 7.1 Hz, 3H) ppm; ^{13}C NMR (DMSO-d_6, 100 MHz, δ) 168.7, 165.9, 158.7, 153.8, 153.7, 144.2, 138.1, 130.1, 121.8, 120.4, 119.2, 116.8, 110.0, 60.2, 20.9, 14.1 ppm; IR (KBr) ν_{max} 2962 (br, w), 1732 (s), 1612 (m), 1371 (m), 1268 (m), 1206 (s), 1144 (s), 1017 (m), 909 (m), 860 (w) cm^{-1}; MS (FAB+, NBA) m/z = 303 (MH^+, 9%); HR-MS (FAB+ of MH^+, NBA; m/z) calcd for $C_{16}H_{15}O_6$ 303.0869, found 303.0862.

Preparation of Acetic Acid 3-Formyl-2-oxo-2*H*-chromen-7-yl Ester (19). Acrylic acid ethyl ester **18** (2.20 g, 7.28 mmol) was dissolved in THF (200 mL). OsO_4 (2 mL of 4% w/w in water) was added to the mixture and stirred for 0.5 h. $NaIO_4$ (3.42 g, 16 mmol) was added, and the suspension was stirred at ambient temperature. Once the starting material was consumed (~5 d), the solution was taken to dryness by rotary evaporation. The resulting solid was partitioned between water and CH_2Cl_2. The organic layer was taken to dryness by rotary evaporation. Product **19** was isolated as a white solid (1.40 g, 83%) using column chromatography (silica−solvent gradient from CH_2Cl_2 to CH_2Cl_2/5% CH_3CN): R_f = 0.54 (silica−CH_2Cl_2/5% CH_3CN); mp = 160−165 °C (dec); ^{1}H NMR (DMSO-d_6, 400 MHz, δ) 10.03 (s, 1H), 8.69 (s, 1H), 8.04 (d, J = 8.5 Hz, 1H), 7.39 (d, J = 2.1 Hz, 1H), 7.26 (dd, J = 8.5, 2.2 Hz, 1H), 2.33 (s, 3H) ppm; ^{13}C NMR (DMSO-d_6, 100 MHz, δ) 188.0, 168.5, 158.9, 155.6, 155.3, 146.3, 132.4, 121.0, 119.4, 116.1, 110.3, 20.9 ppm; IR (KBr) ν_{max} 3115 (m), 3099 (m), 3063 (m), 3041 (m), 3013 (m), 2879 (m), 1766 (s), 1681 (s), 1611 (s), 1563 (s), 1504 (m), 1431 (s), 1373 (s), 1261 (s), 1213 (s), 1196 (s), 1153 (s), 1132 (s), 1038 (m), 1014 (m), 952 (m), 903 (s), 855 (s), 837 (m) cm^{-1}; MS (FAB+, NBA) m/z = 233 (MH^+, 8%); HR-MS (FAB+ of MH^+, NBA; m/z) calcd for $C_{12}H_9O_5$ 233.0450, found 233.0442. Anal. Calcd for $C_{12}H_8O_5$: C, 62.07; H, 3.47. Found: C, 62,11; H, 3.76.

Preparation of Acetic Acid 3-[(Bis(pyridin-2-ylmethyl)amino)methyl]-2-oxo-2*H*-chromen-7-yl Ester (20). To a solution of aldehyde **19** (0.450 g, 1.94 mmol) in 1,2-dichloroethane (50 mL) were added DPA (0.34 mL, 1.89 mmol) and $NaBH(OAc)_3$ (0.82 mg, 3.87 mmol). The reaction was stirred for 12 h at ambient temperature. Saturated aqueous Na_2CO_3 (20 mL) was added to quench the excess reductant, and the mixture was vigorously stirred for 0.5 h. The mixture was partitioned and the aqueous layer further extracted with CH_2Cl_2 (2 × 20 mL). The combined organic extracts were washed with brine (20 mL) and dried over $MgSO_4$. The solvent was removed by rotary evaporation, and **20** was isolated as a brown solid (0.280 g, 36%) using column chromatography (silica−solvent gradient from CH_2Cl_2/40% CH_3CN, over CH_2Cl_2/5% MeOH, to CH_2Cl_2/10% MeOH): R_f = 0.44 (silica−CH_2Cl_2/10% MeOH); mp = 79−83 °C (dec); ^{1}H NMR (DMSO-d_6, 400 MHz, δ) 8.48 (d, J = 4.8 Hz, 2H), 8.15 (s, 1H), 7.77−7.73 (m, 3H), 7.59 (d, J = 7.8 Hz, 2H), 7.24−7.21 (m, 3H), 7.13 (dd, J = 8.4, 2.2 Hz, 1H), 3.85 (s, 4H), 3.60 (s, 2H), 2.30 (s, 3H) ppm; ^{13}C NMR (DMSO-d_6, 100 MHz, δ) 168.8, 160.2, 158.8, 153.0, 152.2, 148.8, 139.5, 136.5, 129.0, 125.2, 122.7, 122.1, 118.5, 117.0, 110.0, 59.6, 52.6, 20.8 ppm; IR (KBr) ν_{max} 1776 (s), 1736 (s), 1613 (s), 1591 (s), 1570 (m), 1498 (m), 1476 (m), 1433 (s), 1367 (s), 1254 (m), 1179 (s), 1143 (s), 1116 (s), 1059 (s), 983 (s), 901 (m), 862 (m) cm^{-1}; MS (ES+, 100% CH_3CN, 30 V) m/z = 416 (MH^+); MS (FAB+, NBA) m/z = 416 (MH^+, 97%); HR-MS (FAB+ of MH^+, NBA; m/z) calcd for $C_{24}H_{22}N_3O_4$ 416.1610, found 416.1629. Anal. Calcd for $C_{24}H_{21}N_3O_4$: C, 69.39; H, 5.10; N, 10.11. Found: C, 69.01; H, 5.14, N, 10.28.

Preparation of 3-[(Bis(pyridin-2-ylmethyl)amino)methyl]-7-hydroxychromen-2-one (21). Ester **20** (0.350 g, 0.84 mmol) was dissolved in MeOH (10 mL). A volume of 10 drops of 0.5 M NaOMe in MeOH was added, and the reaction was stirred for 24 h at ambient temperature. The solvent was removed by rotary evaporation, and **21** was isolated using column chromatography (silica−CH_2Cl_2/5% MeOH) as a white solid (0.190 g, 60% yield): R_f = 0.21 (silica−CH_2Cl_2/10% MeOH); mp = 169−173 °C; ^{1}H NMR (DMSO-d_6, 400 MHz, δ) 10.44 (br s, 1H), 8.47 (d, J = 4.1 Hz, 2H), 8.01 (s, 1H), 7.77−7.73 (m, 2H), 7.58 (d, J = 7.8 Hz, 2H), 7.51 (d, J = 8.5 Hz, 1H), 7.24−7.21 (m, 2H), 6.76 (dd, J = 8.5, 2.2 Hz, 1H), 6.68 (d, J = 2.1 Hz, 1H), 3.82 (s, 4H), 3.54 (s, 2H) ppm; ^{13}C NMR (DMSO-d_6, 100 MHz, δ) 160.8, 160.6, 158.9, 154.5, 148.8, 140.7, 136.5, 129.4, 122.6, 122.1, 120.7, 113.0, 111.5, 101.7, 59.6, 52.6 ppm; IR (KBr) ν_{max} 2812 (br), 1735 (s), 1608 (s), 1477 (m), 1268 (m), 1249 (m), 1115 (m), 1049 (m), 840 (m) cm^{-1}; MS (FAB+, NBA) m/z = 373 (M^+, 10%), 374 (MH^+, 64%); HR-MS (FAB+ of MH^+, NBA; m/z) calcd for $C_{22}H_{20}N_3O_3$ 374.1505, found 374.1510. Anal. Calcd for $C_{22}H_{19}N_3O_3$: C, 70.76; H, 5.13; N, 11.25. Found: C, 70.36; H, 4.99; N, 11.40.

Cell Culture, Fluorescence Microscopy, and in Vitro Evaluation of Chemosensors. For the details of the conditions of the cell culture, the fluorescence imaging procedures used, and the protocols for the in vitro evaluation of the sensors, see the Supporting Information.

Results and Discussion

Choice of Coumarins as Fluorophores. The switch-on signaling event of a chemosensor should be sensitive and selective for the analyte. Sensitivity and selectivity are achieved by a judicious combination of a fluorophore and a metal binding unit. Our fluorophore of choice was 4-(aminomethyl)-6,7-dimethoxycoumarin (**1**). This coumarin is known to be only weakly fluorescing due to a photoelectron transfer (PET) quenching process by the amino group.[65] Hence, conversion to amide **2** generates a strongly fluorescing material.[65]

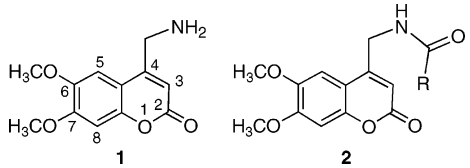

We chose coumarins as fluorophores as they possess excitation/emission wavelengths from 360 up to 550 nm with

Scheme 1 [a]

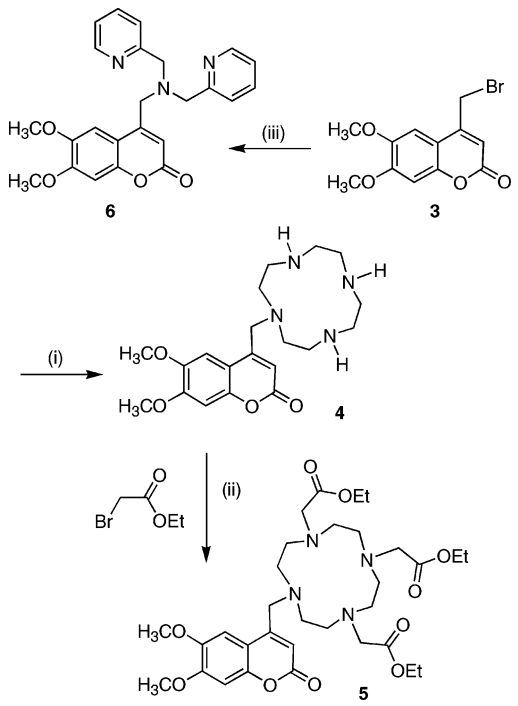

[a] Reaction conditions: (i) cyclen, CH_2Cl_2, Na_2CO_3, 25 °C, 4 d; (ii) CH_2Cl_2, Na_2CO_3, 25 °C, 3 d; (iii) DPA, CH_2Cl_2, Na_2CO_3, 25 °C, 1 d.

extinction coefficients $>18\,000$ cm^{-1} M^{-1} combined with high fluorescence quantum yields.[66] The absorption and emission wavelengths of coumarins are not all in the ideal wavelength regime, i.e., in the green or red portion of the visible spectrum. Longer excitation/emission wavelengths reduce the chances for UV-induced damage to the observed biological systems. However, several hundred derivatives are known or commercially available.[67] The well-studied chemistry of coumarins allows for the variation of all the substituents, thus enabling the careful engineering of the molecular properties of the sensor.[68,69]

Syntheses and in Vitro Evaluation of CHEF-Type Chemosensors 4 and 5. Coumarin-substituted cyclen **4** was synthesized in good overall yield by alkylation of cyclen with stoichiometric amounts of coumarin bromide **3** (Scheme 1). Peralkylation of **4** with ethyl bromoacetate under basic conditions generated triester **5**. The architecture of these fluoroionophores follows the traditional scheme of appending a fluorophore to a polyazamacrocyclic chelator.[19,45,69−71] The cyclen moiety was chosen as a prototype zinc binding site.

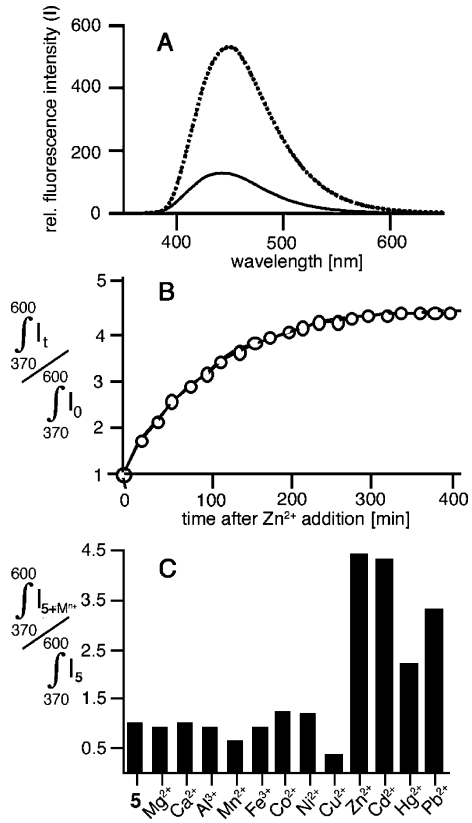

Figure 1. (A) (—) native fluorescence intensity of **5** and (···) addition of 10 equiv of Zn^{2+} (after 12 h, 1 mM **5** in 50 mM PIPES buffer, 100 mM KCl, pH 7). (B) Time course of the integrated fluorescence intensity of **5** after addition of 10 equiv of $ZnCl_2$ (otherwise same conditions as in A). (C) Metal-dependent relative integrated emission intensity increase of **5** (1 μM) in the presence of a 10-fold molar excess of M^{n+} ions, as their chlorides ($\lambda_{ex} = 345$ nm; $Zn^{2+} \equiv 1.0$; 50 mM HEPES buffer, pH 7, 100 mM KCl, 10 μM EDTA, 30 h). Conditions: $\lambda_{ex} = 345$ nm; 25 °C; aerated solutions in all cases.

Both assemblies **4** and **5** possessed the expected spectroscopic and analytical properties.

The UV−vis ($\lambda_{max} = 345$ nm) and fluorescence spectra ($\lambda_{max} = 446-448$ nm) of sensors **4** and **5** are nearly identical. Upon addition of Zn^{2+}, **5** shows a 4.4-fold increase in its emission intensity (Figure 1A; as will later be detailed, sensor **4** is not taken up by live cell cultures, hence only sensor **5** will be discussed in detail). The quantum yield ϕ for the complex **5**·Zn^{2+} was determined to be 0.26 (ϵ_{345nm} for **5**·Zn^{2+} = 9200 cm^{-1} M^{-1}).[72] Protonation of the ring nitrogens also causes a fluorescence increase, but this becomes prominent only at a pH below 4. Hence, the sensor is suitable for use under physiological conditions. A Hill plot demonstrates the expected 1:1 stoichiometry of metal to sensor. The dissociation constant K_d of this complex was estimated to be in the order of 1 μM in a 1,4-piperazinebis(ethanesulfonic acid) (PIPES) buffer at pH 7. The binding of **5** to Zn^{2+} is, however, slow (Figure 1B). This likely reflects the considerable reorganization energy required to make the

(65) Sasamoto, K.; Ushijima, T.; Saito, M.; Ohkura, Y. *Anal. Sci.* **1996**, *12*, 189−193.
(66) Koller, E.; Fauler, G. *Appl. Fluoresc. Technol.* **1992**, *4*, 18−24.
(67) (a) Estevez-Braun, A.; Gonzalez, A. G. *Nat. Prod. Rep.* **1997**, *14* (5), 465−475. (b) O'Kennedy, R., Thornes, R. D., Ed. *Coumarins: Biology, Applications and Mode of Action*; Wiley: Chichester, U.K., 1997. (c) *Flavonoids & Coumarins Catalogue*; The Indofine Chemical Co., Inc.: Hillborough, NJ, 2003. (d) *Fluorescent Probes Catalogue*; Fluka Riedel-de Haën: Milwaukee, WI, 2004. (e) Reference 84.
(68) Pharmaceutically active coumarin derivatives were recently reviewed: (a) Pochet, L.; Frederick, R.; Masereel, B. *Curr. Pharm. Des.* **2004**, *30*, 3781−3796. (b) Lacy, A.; O'Kennedy, R. *Curr. Pharm. Des.* **2004**, *30*, 3797−3811. (c) Fylaktakidou, K. C.; Hadjipavlou-Litina, D. J.; Litinas, K. E.; Nicolaides, D. N. *Curr. Pharm. Des.* **2004**, *30*, 3813−3833. (d) Reference 69.
(69) Katerinopoulos, H. E. *Curr. Pharm. Des.* **2004**, *30*, 3835−3852.
(70) Akkaya, E. U.; Huston, M. E.; Czarnik, A. W. *J. Am. Chem. Soc.* **1990**, *112*, 3590−3593.
(71) Nishimura, G.; Shiraishi, Y.; Hirai, T. *Ind. Eng. Chem. Res.* **2004**, *43*, 6064−6069.
(72) Measured against Eosin Y in basic EtOH: Seybold, P. G.; Gouterman, M.; Callis, J. *Photochem. Photobiol.* **1969**, *9*, 229−242.

peripherally substituted and, therefore, rigidified cyclen moiety available for metal binding. Correspondingly, sensor **4** binds Zn(II) instantaneously. Surprisingly, the slow binding of **5** does not impose restrictions for the utility of this sensor to trace zinc in live cells (see below). The selectivity of the fluorescence increase upon exposure of sensor **5** to a 10-fold excess of a variety of metal ions is shown in Figure 1C.

The sensor is inert toward a range of ions. Parallel to many "zinc-specific" sensors, however, Cd^{2+}, and, to a lesser extent, Pb^{2+} and Hg^{2+} result in a switch-on response.[25,73] However, the concentration of these toxic heavy metal ions is expected to be low in healthy cells. The ions Cu^{2+} and Mn^{2+} are also expected to bind to the cyclen moiety, but these paramagnetic ions quench any chelation-induced fluorescence, excluding a false positive signaling for zinc. It is interesting to note that the related chelate DOTA (cyclen *N*,*N*′,*N*″,*N*‴-tetraacetic acid) binds Ca^{2+}, whereas **5** shows no appreciable binding.[74] Thus, the selectivity profile for **5** is appropriate for its use as a zinc-specific sensor in biological media.

Synthesis and in Vitro Evaluation of CHEF-Type Chemosensor 6. Since binding of **5** to Zn^{2+} was slow, we changed the polyazamacrocycle metal recognition unit to a more flexible open-chain binding site. Bis(2-picolyl)amine (DPA) has been shown to have a good affinity for Zn^{2+} and, consequently, was previously used in zinc-selective chemosensor designs.[19,28,54] Coumarin-substituted DPA **6** was synthesized in excellent yield by reaction of DPA with coumarin bromide **3** (Scheme 1). Isolation and purification of **6** was accomplished by column chromatography, representing a great advantage over the preparation of cyclen-based sensor **5**. The constitution of **6** could convincingly be deduced from its spectroscopic and analytical data.

Figure 2A shows the excellent chemosensory response of sensor **6**. Addition of 1 equiv of Zn^{2+} increases the integrated fluorescence intensity 22-fold. This CHEF-type increase compares favorably to that of many known zinc-specific chemosensors, save for Zinquin and rare other examples.[43,75] The fluorescence quantum yields ϕ for **6** and **6**·Zn^{2+} in MeOH are 0.04 and 0.88,[76] respectively (ϵ_{343nm} for **6** and **6**·Zn^{2+} in MeOH are 7600 and 6800 cm^{-1} M^{-1}, respectively). Comparing the switching behavior of **5** and **6**, one notices that both sensors are similarly "switched off" in the free base state but that the DPA-based sensor **6** is subject to a stronger "switching on" behavior upon coordination to Zn^{2+}. The extinction coefficient together with the fluorescence quantum yield result in a satisfactory brightness of sensor **6**. Even visual inspection of vials containing solutions of **6** with and without Zn^{2+} under ambient and UV light allows their distinction by observation of the induced fluorescence (see image used in the Table of Contents Synopsis). As expected, the binding of **6** to Zn^{2+} is fast and completed upon mixing

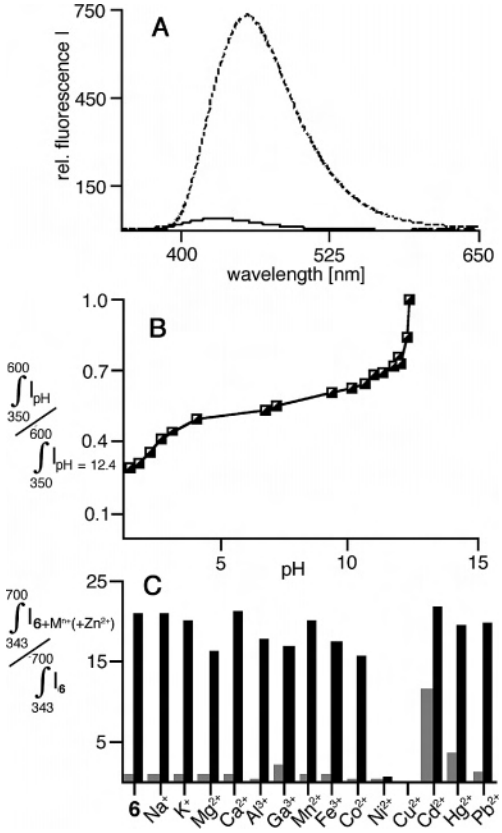

Figure 2. (A) (—) Native fluorescence intensity of **6** and (···) addition of 1 equiv of Zn^{2+} (conditions: [**6**] = 192 μM in MeOH). (B) Plot of the integrated emission intensity versus pH ([**6**] = 1 μM in H_2O containing 1 mM KOH and 100 mM KCl, pH adjusted with 1.0 M HCl (dilution during the titration was negligible)). (C) M^{n+}-selectivity profile of sensor **6**: light bars, relative integrated emission intensity of **6** + 1 equiv of M^{n+} (as their chlorides); solid bars, relative integrated emission intensity of **6** + M^{n+} (as their chlorides), followed by 1 equiv of Zn^{2+}. Conditions: [**6**] = 163 μM in MeOH; $\lambda_{excitation}$ = 343 nm; 25 °C; aerated solutions in all instances.

Table 1. Solvent-Dependent Relative Fluorescence Increase and Apparent Binding Constant Measured for Sensor **6** (Concentrations Ranging from 0.8 to 1.9 10^{-4} M)

solvent	intensity increase $\int_{350}^{650} I_{\mathbf{6}+Zn} \Big/ \int_{350}^{650} I_{\mathbf{6}}$	apparent K_d (μM)
$CHCl_3$	15	2.0
80:20 DMSO−H_2O	11	55
50:50 DMSO−H_2O	23	0.67
10:90 MeOH−H_2O	23	8.0
MeOH	22	0.50

of ligand and metal. The zinc-induced relative fluorescence increase of **6** and the apparent K_d are solvent dependent. The more polar (aqueous) the solvent system, the larger the relative fluorescence increase (Table 1). No trend can be recognized in the solvent dependency of the K_d for the zinc complex **6**·Zn^{2+}.

Sensor **6** forms a 1:1 complex with Zn^{2+} (Hill plot analysis) and is suitable for measurements in aqueous media of pH 4−11 (Figure 2B). The apparent K_d of the complex is in the order of 0.5 μM (MeOH). This value is high compared to other DPA-based sensors.[28,54] It should be noted, however, that we determined the K_d photometrically using a 1:1 metal: ligand binding model and did not use the potentiometric titration methods more commonly used. Figure 2C plots the

(73) Costero, A. M.; Gil, S.; Sanchis, J.; Peransi, S.; Sanza, V.; Williams, J. A. G. *Tetrahedron* **2004**, *60*, 6327−6334.
(74) Clarke, E. T.; Martell, A. E. *Inorg. Chim. Acta* **1991**, *190*, 27−36.
(75) Hirano, T.; Kikuchi, K.; Urano, Y.; Higuchi, T.; Nagano, T. *Angew. Chem., Int. Ed.* **2000**, *39*, 1052−1054.
(76) Measured against quinine sulfate in 0.1 M H_2SO_4.[62]

Scheme 2 [a]

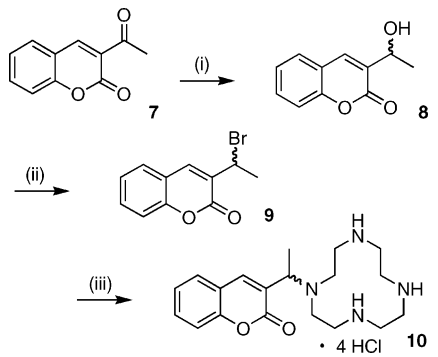

[a] Reaction conditions: (i) $CeCl_3$, $NaBH_4$/THF, 0 °C, 2 h; (ii) PBr_3/benzene, 25 °C, 2 h; (iii) cyclen, CH_2Cl_2, Na_2CO_3, 25 °C, 2 h.

results of a metal binding competition study. The fluorescence of **6** in the presence of a range of metal ions in the absence and the presence of 1 equiv of Zn^{2+} is plotted. While a range of metals bind to the sensor, addition of 1 equiv of Zn^{2+} outcompetes all but Ni^{2+} and Cu^{2+}. The paramagnetic ions Ni^{2+} and Cu^{2+} remain bound but,[77] again, due to their quenching properties, these ions will not provide a false positive signal mimicking the presence of Zn^{2+}. This finding is in accord with the higher binding constants of Ni^{2+} (K_1 = 8.70) and Cu^{2+} (K_1 = 9.31) for the parent chelate DPA as compared to that of Zn^{2+} (K_1 = 7.57).[78] It is of note that, unlike sensor **5**, sensor **6** shows a higher selectivity for Zn^{2+} over Cd^{2+}, reflecting the higher affinity of DPA to Zn^{2+} (K_1 of DPA for Cd^{2+} = 6.44).[78] Taken all results together, they demonstrate the competence of sensor **6** for the determination of zinc in the presence of a range of biologically relevant metal ions. For the evaluation of this sensor in cell cultures, see below.

Shifting the Cyclen Attachment Point on the Coumarin. The signal derived from a fluorescence microscopy image of a cell stained with a zinc-specific chemosensor allows the determination of the presence of zinc. Relative fluorescence emission intensities can reasonably be correlated with increases in $[Zn^{2+}]$, especially when the intensity has been shown to be modulated by externally induced changes of zinc availability. However, the fluorescence quantum yield ϕ of a fluor is generally solvent-dependent. Since the solvent properties of the local environments in which the sensors accumulate in the cell are not known, the absolute $I_{emission}$ measured cannot be correlated with a particular $[Zn^{2+}]$. The measurement of absolute $[Zn^{2+}]$, however, can be achieved using a ratiometric sensor.[62]

One design paradigm for the synthesis of ratiometric sensors is to involve the chromophore in the coordination interaction with Zn^{2+} so as to perturb its electronic structure.[32,34,54] The lactone carbonyl in coumarins is a potential donor atom attached to the chromophore, but sterics prevent the lactone oxygen in sensors **5** and **6** from participating in the coordination event. Moving the aminomethyl attachment point of the chelating moiety on the coumarin from the 4- to the 3-position potentially allows for carbonyl participation. Thus, we synthesized sensor assembly **10** (Scheme 2). Reduction of the readily available 3-acetylcoumarin **7** under Luche's condition ($NaBH_4$, $CeCl_3$) produced the secondary alcohol **8** without concomitant reduction of the lactone. Bromination of **8** with PBr_3 generated bromocoumarin **9**. Using the same methods as for the synthesis of sensor **4**, cyclen was alkylated with **9**.

However, upon addition of Zn^{2+}, ligand **10** displays only ~2-fold increase in fluorescence intensity with no significant shift in $\lambda_{emission}$ (see Supporting Information). This led us to conclude that the lactone carbonyl oxygen does not get involved in the coordination event. This may indicate that the Lewis acidity of the cyclen-coordinated Zn^{2+} is not pronounced enough to strongly coordinate to the lactone oxygen,[79] which in itself is not a particularly good donor atom. This supposition suggests the synthesis of an improved system by limiting the number of coordinating atoms in the metal recognition unit, thereby causing a coordinatively unsaturated zinc center. This then would presumably force the coumarin lactone group to coordinate. Further, a negative steric influence of the methyl group located adjacent to the linking carbon cannot be excluded. The weak fluorophoric response upon zinc chelation to **10** provides an important fundamental piece of knowledge for the design of chemosensors, namely that the PET-fluorescence quenching effect of an aminomethyl group attached to the 3-position of the coumarin may not be as efficient as compared to coumarins derivatized in the 4-position. The profound change in the fluorescent properties of coumarins upon shifting the substituents is known.[80] This, however, may not be at all a disadvantage for the realization of a ratiometric sensor because a large CHEF-type response may obscure any wavelength shift of λ_{max-em} upon zinc binding (see, for instance, below the discussion of sensors **20** and **21**).

Synthesis and Spectroscopic Evaluation of Ratiometric Sensor 15. Following the design rationales outlined above, we proceeded to synthesize the DPA-substituted coumarin **15** by reductive amination of coumarin aldehyde **14** with DPA (Scheme 3). Key intermediate **14** was synthesized starting from *m*-anisidine **11**. Following conversion of **11** to julolidine aldehyde **12** in three steps,[64] a Knoevenagel-type condensation of **12** with glutaconate provided coumarin derivative **13**. OsO_4-induced cis-dihydroxylation and in situ oxidative diol cleavage of **13** afforded coumarin-3-aldehyde **14** in good overall yield.[81] The spectroscopic and analytical data for **15** and its precursors confirm their assigned structures.

(77) Experiments in which 1 equiv of Ni^{2+} or Cu^{2+} was added to a 200 μM solution of (nonbinding) **2** in MeOH indicated that the effects of the paramagnetic contact quenching of the fluorescence are almost negligible, thus proving that the fluorescence quenching observed is due to bound ions.

(78) Romary, J. K.; Barger, J. D.; Bunds, J. E. *Inorg. Chem.* **1968**, *7*, 1142−1145.

(79) For representative examples of the utilization of the Lewis acidity of cyclen-coordinated Zn^{2+}, see: (a) Aoki, S.; Shiro, M.; Koike, T.; Kimura, E. *J. Am. Chem. Soc.* **2000**, *122*, 576−584. (b) Subat, M.; Borovik, A. S.; König, B. *J. Am. Chem. Soc.* **2004**, *126*, 3185−3190.

(80) Bursulaya, B. D.; Druzhinin, S. I.; Uzhinov, B. M. *J. Photochem. Photobiol., A* **1995**, *92*, 163−172.

(81) Padmanabhan, S.; Peri, R.; Triggle, D. J. *Synth. Commun.* **1996**, *26*, 827−831.

Scheme 3 [a]

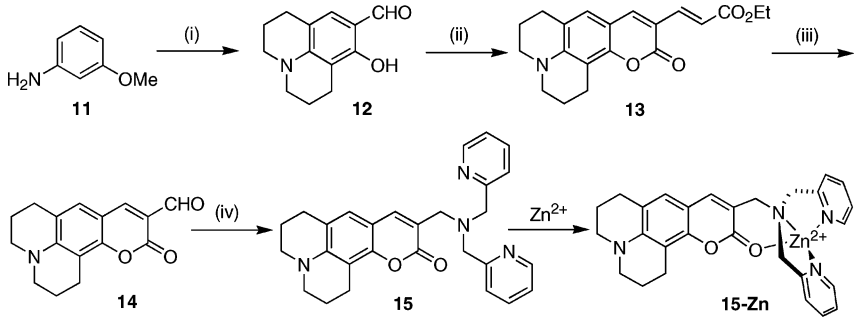

[a] Reaction conditions: (i) (step 1) 1-bromo-3-chloropropane, Na_2CO_3, Δ, 12 h, (step 2) BBr_3/CH_2Cl_2, Δ, 1 h, followed by $MeOH/H_2O$, (step 3) $POCl_3$/DMF, 100 °C, 30 min, followed by aqueous workup;[64] (ii) diethylglutaconate/EtOH, catal piperidine, Δ, 1 d;[81] (iii) $OsO_4/NaIO_4$, THF, 25 °C, 5 d;[81] (iv) DPA, $NaBH(OAc)_3$, $ClCH_2CH_2Cl$, 25 °C, 1 d.

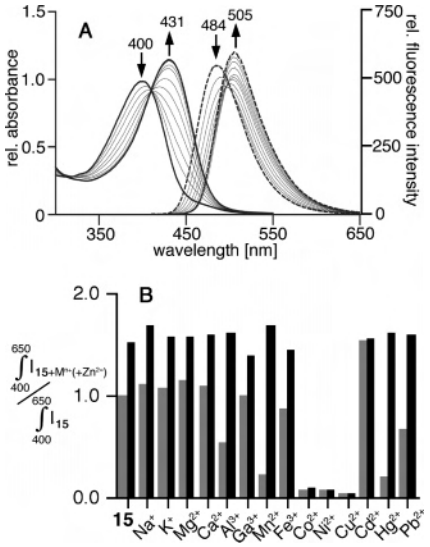

Figure 3. (A) (—) UV−vis spectral titration of **15** with Zn^{2+} (0−1 equiv) and (···) fluorescence response upon titration of **15** with Zn^{2+} (0−1 equiv). Conditions: [**15**] = 100 μM in MeOH; $\lambda_{excitation}$ = 410 nm (isosbestic point). (B) M^{n+}-selectivity profile of sensor **15**: light bars, relative integrated emission intensity of **15** + 1 equiv of M^{n+}; solid bars, relative integrated emission intensity of **15** + M^{n+}, followed by 1 equiv of Zn^{2+}. Conditions: [**15**] = 199 μM in MeOH; $\lambda_{excitation}$ = 396 nm; 25 °C; aerated solutions.

The results of a spectrophotometric titration of the DPA derivative **15** with Zn^{2+} are shown in Figure 3A. In stark contrast to sensor **6** (or sensor **10**), **15** exhibits only minimal CHEF-type behavior. Most significantly, however, the 31 nm shift of the $\lambda_{max-absorption}$ upon addition of Zn^{2+} demonstrates the metal ion-induced perturbation of the chromophore electronic structure. Hence, a ratiometric fluorescence response can be expected. This is indeed observed. Incremental additions of Zn^{2+} result in a 21 nm bathochromic shift of the $\lambda_{max-emission}$ of **15**·Zn^{2+} (λ_{ex} at the isosbestic point at 410 nm). This shift is solvent-dependent and is minimized in solvent systems containing increasing amounts of water (e.g. using $\lambda_{excitation}$ at 412 nm in 80:20 DMSO−H_2O showed a shift in λ_{max-em} from 483 to 508 nm; using λ_{ex} = 417 nm in 50:50 DMSO−H_2O, the shift of λ_{max-em} is only from 494 to 513 nm, and the peak separation is barely discernible). We suggest the structure shown in Scheme 3 for **15**·Zn^{2+}. The fourth coordination site of the N_3O-tetrahedrally coordinated metal center is provided by the lactone oxygen, though the formation of a pentacoordinated metal center by inclusion of another water or alcohol cannot be excluded.[25] In fact, the solvent-dependency of the $\lambda_{max-emission}$ shift suggests that water is competing with the carbonyl oxygen for coordination to the metal center.

Sensor **15** in its free base form is already "switched on", with a ϕ of 0.64 (ϵ = 16900 cm^{-1} M^{-1}, MeOH).[82] This appears to be a further confirmation of the finding that a methyleneamino group attached to the 3-position of the coumarin does not quench the fluorescence of the chromophore effectively.[80] Therefore, chelation results only in a minimal increase of the fluorescence intensity. Ligand **15** is suitable for applications under physiological conditions. The fluorescence response does not change significantly in the range from pH 4−11.[83]

The metal selectivity of the sensor, as shown in the competition with a range of metal ions, is generally in line with previous observations of DPA-based sensors and, thus, appropriate for its intended application (Figure 3B). In a comparison of the metal-dependent response of the two DPA-based sensors **6** and **15**, some differences are of note. Unlike sensor **6**, **15** binds Co^{2+} very well. This is likely a reflection of the more flexible tetrahedral N_3O chelate site provided in **15**. In line with this assumption, **15** also binds the larger Cd^{2+} ion more strongly than **6**.

Influence of a Shift of a Tautomeric Equilibrium in the Sensor upon Coordination to Zn^{2+}. The results reported above show the principle validity of the design paradigm for a ratiometric sensor and point toward the synthesis of improved ratiometric sensors. One aspect in the realization of a drastic ratiometric response of a chemosensor appears to be the shifting of a phenol−quinone-type tautomeric equilibrium as shown for the 6-hydroxycoumarin chromophores **I** and **II** (Figure 4). An equivalent equilibrium shift was first evoked by Lippard and co-workers to rationalize the ratiometric behavior (or lack thereof) in their sensors.[32,54] Considering sensor **15**, it can reasonably be expected that coordination of zinc to the lactone carbonyl also affects the imine−enamine equilibrium (**III** and **IV**) with the important difference that iminium form **IV** carries a positive charge (and causes a large charge separation) which cannot be

(82) Measured against diphenylanthracene in cyclohexane.[62]
(83) The fluorometric method we used to determine K_d (see Supporting Information) is not suited to measure the K_d of a sensor exhibiting a significant wavelength shift upon binding.

Scheme 4 [a]

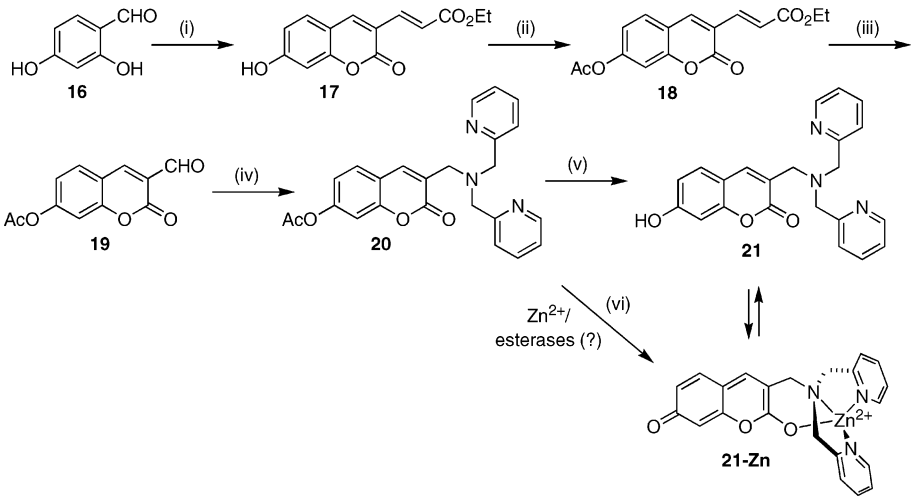

[a] Reaction conditions: (i) diethylglutaconate, EtOH, catal piperidine, Δ, 1 d;[64,81] (ii) Ac_2O/pyridine; (iii) $OsO_4/NaIO_4$, THF, 25 °C, 5 d;[81] (iv) DPA, 2 equiv of $NaBH(OAc)_3$, $ClCH_2CH_2Cl$, 25 °C, 1 d; (v) NaOMe/MeOH, 25 °C, 1 d; (vi) Zn^{2+}, solvent.

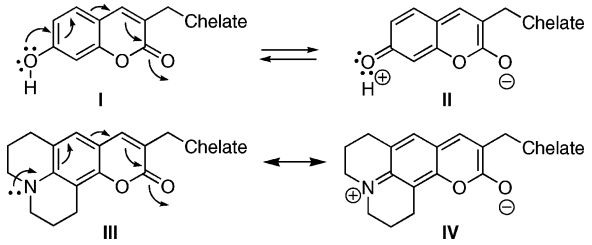

Figure 4. Proposed tautomeric/resonance forms modulating the photophysical properties of the chromophore.

relieved by deprotonation (as in **II**) (Figure 4). What is the effect of these types of equilibria on the ratiometric response of coumarin-based chemosensors? An answer of this question may help to further define the designs of single-dye ratiometric sensors.

We therefore synthesized sensors **20** and **21**, the oxygen-analogues to sensor **15** (Scheme 4) Whereas sensor **21** can undergo a tautomeric shift (**I** ⇄ **II**), its acetylated form **20** cannot. Thus, comparison of the response profile of sensors **15**, **20**, and **21** should allow the verification of the influence of the 7-coumaryl substituents, their possible tautomeric forms on their zinc-induced switching behavior, and the quantification of any effect.

The synthesis of **20** follows broadly the same lines as that of **15**. A coumarin chromophore (**17**) is constructed from an appropriately substituted benzaldehyde (**16**) using well-known cyclization reactions.[64] Acetylation to form **18** is followed by oxidative olefin cleavage to furnish the key compound **19**.[81] Aldehyde **19** is set up for reductive amination with DPA, producing **20** which, upon base-catalyzed deacetylation, generates sensor **21**. All the synthetic steps proceeded smoothly and all products allowed their unequivocal identification by spectroscopic and analytical means.

Figure 5 shows the results of the spectrophotometric and fluorometric titration of **20** and **21** with zinc in four different solvents. Much to our surprise, both sensors exhibited a strong CHEF-type response in all solvents investigated (e.g. 97-fold for **21** in $CHCl_3$ at 409 nm). This invalidates the hypothesis derived earlier that methyleneamino functionalities attached to the 3-position as opposed to the 4-position do not effectively quench the native fluorescence of coumarins by means of a PET process. Apparently, the explanation for the observed effects are much more intricate and involve the nature of the substituents on the 6- and 7-positions on the chromophore.[80]

UV−vis titration of **20** with Zn^{2+} in all solvents shows only minor changes in λ_{max} or the extinction coefficient ϵ, indicating that zinc-binding to the sensor causes only minor electronic perturbations (Figure 5A,C,E,G; for all optical data, see Table 2). In contrast, titration of **21** in all solvents shows a larger shift of λ_{max} (e.g. 17 nm shift in $CHCl_3$, Figure 5B), although still not as large as observed for the ratiometric sensor **15** (Figure 3A). This suggests only a minor shift of $\lambda_{max-emission}$ in the fluorescence spectra of both sensors **20** and **21** upon coordination to zinc. This is largely true for the spectra of **20** and **21** in $CHCl_3$ and DMF (Figure 5A−D). However, the surprisingly large CHEF-type fluorescence enhancement of the signals obscures even large wavelength shifts. For instance, $\lambda_{max-emission}$ of **21** is at 472 nm whereas $\lambda_{max-emission}$ of **21**·Zn is at 407 nm (Figure 5D). The close similarity of the spectra for acetyl derivative **20** and phenol **21** in these solvents suggests that the zinc complex occurs predominantly in the phenol-tautomeric form **I**. The fluorescence response of **20** and **21** in MeOH and H_2O (Figure 5E−H) varies dramatically from those in the nonprotic solvents. Sensor **21** in MeOH, for example, exhibits, next to the peak at 408 nm we interpret as indicative for the phenol-tautomeric form **I**, a second peak at 472 nm (Figure 5F). This may be a sign for the occurrence of the quinone-form **II**. Sensor **20** shows a shoulder around 470 nm. This shoulder is stable over time, but the attribution of this shoulder to small amounts of (slow) hydrolysis cannot be excluded. The species giving rise to the peak at 471/472 nm is the sole species observed for **21** in H_2O (Figure 5H). The fluorimetric titration of acetoxy-species **20** with zinc in H_2O also shows the appearance of two peaks (Figure 5G). However, the signal shifts over time (∼24 h at 25 °C) to that derived from the titration of **21** in water (Figure 5H).

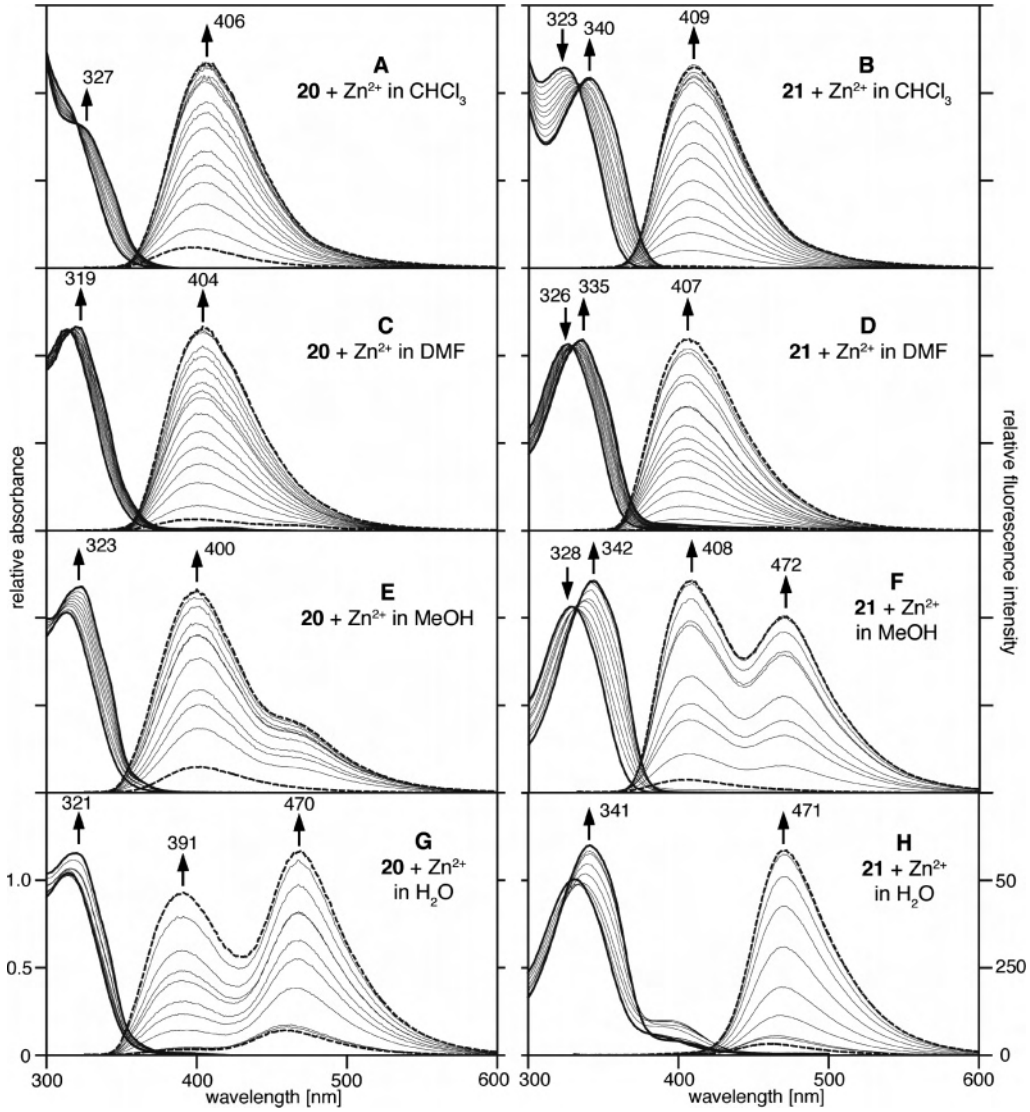

Figure 5. (—) UV−vis spectral titrations of **20** and **21** with Zn^{2+} (0−1 equiv), respectively, and (···) fluorescence response upon titration of **20** and **21** with Zn^{2+} (0−1 equiv, as its chloride salt in MeOH) in the solvents indicated. Conditions: $\lambda_{excitation}$ at isosbestic point or $\lambda_{max-\mathbf{20/21}}$ (A, $\lambda_{excitation}$ = 320 nm; B, $\lambda_{excitation}$ = 333 nm; C, $\lambda_{excitation}$ = 315 nm; D, $\lambda_{excitation}$ = 329 nm; E, $\lambda_{excitation}$ = 318 nm; F, $\lambda_{excitation}$ = 332 nm; G, $\lambda_{excitation}$ = 318 nm; H, $\lambda_{excitation}$ = 330 nm); [**20**]/[**21**] = 100 μM; 25 °C; aerated solutions.

Table 2. Solvent-Dependent Relative UV−Vis and Fluorescence Properties and Apparent Binding Constant Measured for Sensors **20** and **21** (at Concentrations of 100 μM)

solvent	sensor	λ_{max} (ϵ) for sensor, λ_{max} (ϵ) for sensor·Zn^{2+} [nm (cm^{-1} M^{-1})]	λ_{max-em} for sensor, λ_{max-em} for sensor·Zn^{2+} (nm)	rel fluorescence intensity increase	fluorescence quantum yield: sensor, sensor·Zn^{2+}	apparent K_d (μM)
$CHCl_3$	20	311 (15 000), 327 (12 500)	399, 406	9[a]	n/d	0.82
	21	323 (16 700), 340 (15 800)	398, 409	97[a]	n/d	6.5
DMF	20	314 (11 200), 319 (11 400)	403, 404	11[a]	n/d	7.6
	21	326 (16 500), 335 (17 000)	461, 407	31[a]	n/d	25.6
MeOH	20	313 (11 400), 323 (12 800)	399, 400	9[a−c]	0.057, 0.52	3.1
	21	328 (13 500), 342 (15 400)	406, 408/472	24[a,b]	0.034, 0.81	3.6
H_2O	20	315 (10 900)	391/470 (hydrolysis)	hydrolysis	0.037, 0.41	6.0
	21	330 (11,800), 341 (13,700)	459, 471	18[a,b]	0.04, 0.73	3.1

[a] Determined by $\int_{350}^{600} I_{\mathbf{20/21}+Zn^{2+}} \Big/ \int_{350}^{600} I_{\mathbf{20/21}}$. [b] Determined by $\phi_{sensor\cdot Zn^{2+}}/\phi_{sensor}$. [c] Partial hydrolysis.

We interpret that result as a sign for the hydrolysis of the acetyl functionality. In support of this, in ESI-MS of an aqueous solution of **20** containing zinc, the mass peak for **21** becomes prominent over time. The acetyl-protected sensor may be of advantage in any in vivo or in cyto application of the sensor. Intracellular esterases and/or intracellular zinc may liberate **21** from its more lipophilic prodrug form **20**.

The effects of *O*-alkylation of the 7-OH group of umbelliferones (7-OH coumarins) on their fluorescence properties have been studied. For instance, the 7-*O*-gluco- and galac-

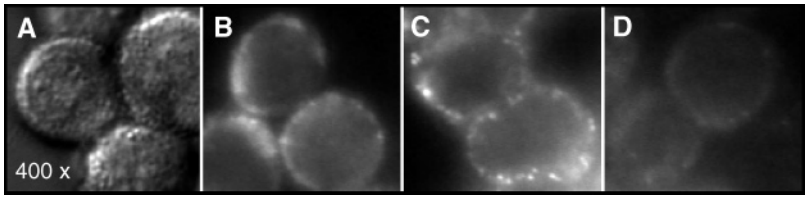

Figure 6. (A) Light and (B−D) fluorescence micrographs of cultured GH3 rat pituitary tumor cells incubated with **5**: (B) cells incubated with **5**; (C) cells incubated with **5** + Zn^{2+} (50 μM) + pyrithione (20 μM); (D) **5** + TPEN (100 μM). Conditions: for cell culture and fluorescence imaging conditions, see the Supporting Information.

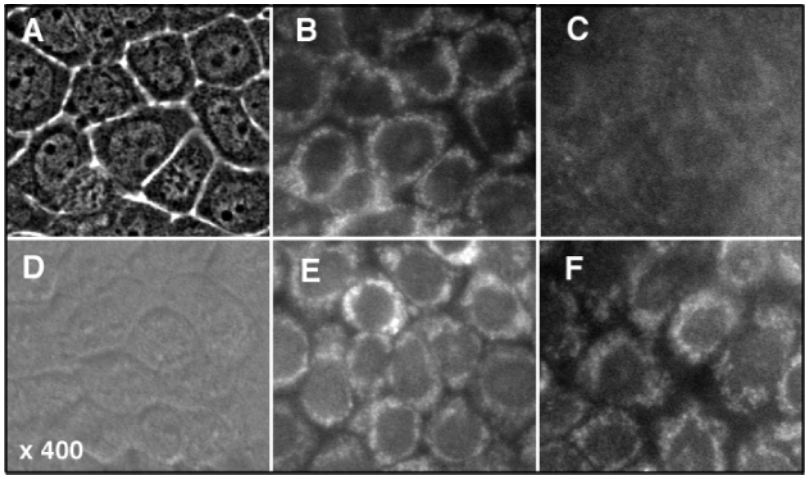

Figure 7. (A) Light and (B−F) fluorescence micrographs of cultured H4IIE hepatoma cells: (B) incubated with **6** + Zn^{2+} (50 μM) + pyrithione (20 μM); (C) cells of (B) after treatment with TPEN (100 μM); (D) cells incubated with Zn^{2+} (50 μM) + pyrithione (20 μM) and no sensor (image brightness greatly enhanced to show outlines of cells); (E) incubated with **15** + Zn^{2+} (50 μM) + pyrithione (20 μM); (F) cells of (E) after treatment with TPEN (100 μM). Conditions: for cell culture and fluorescence imaging conditions, see the Supporting Information.

topyranoside derivatives of coumarins do not fluoresce, whereas the 7-*O*-dealkylated derivatives fluoresce strongly (when present in the deprotonated form).[84] This reaction is the basis for a number of galactosidase and glucosidase assays.[84] The findings in this study which differ from the known effects in umbelliferones are that fluorescence can also be switched on in an 7-*O*-acyl species (**20**) by metal coordination to an 3-aminomethyl group (and, likely, concomitant to the 1-oxo group). In general, the observed complex modulation pattern of the photophysical properties of the coumarins upon changes of the peripheral substitution pattern is in line with literature-known observations.[69]

Biological Evaluation of the Sensors 4−6 and 15. For the biological evaluation of our sensors we chose two different cell lines, GH3 rat pituitary tumor cells and H4IIE cells, a rat hepatoma cell line. The former was chosen to build on earlier work investigating the effects of zinc availability on thyroid hormone action.[12−14] The latter widely used hepatoma cell line was also chosen because the GH3 cells used possess an unusual morphology and the differentiation of subcellular compartments is difficult. In addition, the liver is an organ of interest with respect to zinc homeostasis and action.

Cultured GH3 rat pituitary tumor cells of varying zinc status were incubated with sensors **4** and **5** and the cells inspected under a fluorescence microscope (Figure 6). The results were compared to staining experiments using untreated controls. Only the ester derivatives **5** resulted in fluorescent cells. The pendant esters probably turn the chelates into more lipophilic prodrugs. Once passively diffused into the cell, esterases may cleave the esters and the resulting carboxylates are retained in the cell, leading to sustained staining. Such a mechanism has also been shown to operate for Zinquin esters.[44] The fluorescence did not diminish over 120 min.

A standard set of experiments was performed to link the staining to intracellular zinc pools and to minimize the potential for having artifacts such as the observation of the weakly fluorescing (but not nonfluorescing) sensor itself:[22] (a) The cells show no fluorescence in the absence of the sensor. (b) The observed stains were sensitive to an exogenously altered zinc status of the cell. Addition of the ionophore pyrithione (2-mercaptopyridine *N*-oxide) in conjunction with added Zn^{2+} is known to load the cells with zinc. Correspondingly, the observed fluorescence intensity of the stains increased dramatically (cf. Figure 6 part B with part C). Inversely, the addition of the cell permeable zinc scavenger *N*,*N*,*N*′,*N*′-tetrakis(2-picolyl)ethylenediamine (TPEN)[23,25] reduced the intracellular zinc availability and, therefore, the observed fluorescence diminished (Figure 6D). (c) Incubation of the cells with trypan blue demonstrated that the cells remained viable during these treatments. (d) The staining was also shown not to be due to sensor−zinc complexes preformed outside of the cell. Thus, incubation of cells with the sensor−zinc complex did not result in any staining. This can be rationalized considering the dipositive charge of the

(84) Haugland, R. P. *Handbook of Fluorescent Probes and Research Chemicals*, 9th ed.; Molecular Probes: Eugene, OR, 2002.

sensor−zinc complex, preventing uptake by diffusional processes. The cell culture experiments suggest faster zinc-binding kinetics by the sensor than observed in vitro. This apparent conflict with the in vitro findings is as yet unexplained but may be due to the presence of the sensor in a preorganized medium such as a lipid membrane structure.

Both sensors **6** and **15** are competent imaging agents for zinc in GH3 rat pituitary tumor cells (not shown) as well as rat H4IIE cells (Figure 7). Using the protocols described above, punctate staining was observed (Figure 7B,E). Cells incubated with the pyrithione and zinc did not fluoresce in the absence of a sensor (Figure 7D). Whereas the fluorescence diminished upon addition of TPEN to the cell cultures incubated with CHEF-type sensor **6** (Figure 7C), the cells continue to fluoresce when using sensor **15** (Figure 7F). This is because the ratiometric sensor **15** is fluorescent irrespective whether zinc is present or not. The potential ratiometric capabilities of sensor **15**, however, were not utilized.

Conclusions

In conclusion, coumarin-based chemosensors are competent zinc-specific sensors of utility in biological systems. Further, the readily modified coumarin moiety provides a platform for the synthesis of chemosensors aiming at answering fundamental questions regarding the design of chemosensors. This said, however, the question as to what effects a shift of a tautomeric equilibrium has on the fluorophoric response profile of a chemosensor cannot be answered simplistically. While it is clear that the effect is large, suggesting the further exploration of sensors trying to take advantage of shifting such equilibria, the overall effects of the change of substitution pattern on the coumarin **20**/**21** compared to that of **15** also had unexpected (and perhaps domineering) effects with respect to the change in the CHEF-type response of the sensor. We are currently studying further variations in the substitution patterns to continue defining the design algorithm of coumarin-based chemosensors in specific and, more importantly, chemosensors in general.

Acknowledgment. We thank Michelle Barber (Flow Cytometry and Confocal Imaging Facility, UConn Biotechnology Center/Molecular and Cell Biology) for technical assistance. This work was supported by the UConn Research Foundation (C.B. and H.C.F.) and the Petroleum Research Fund (Grant PRF-37432-G1), administered by the American Chemical Society (C.B.). J.V.S. thanks the National Science Foundation for an NSF-REU summer research stipend, and M.C.P. acknowledges a Pfizer/CBIA fellowship.

Supporting Information Available: Experimental details of the in vitro and cell studies, ^{1}H and ^{13}C NMR spectra of **4**−**6**, **10**, **13**−**15**, and **17**−**21**, tables of the photophysical data for **6** and **6**·Zn^{2+}, and those pH- and solvent-dependent fluorescence titration curves of the sensors **4**−**6**, **10**, **15**, **20**, and **21** which were not included here. This material is available free of charge via the Internet at http://pubs.acs.org.

IC048905R